International Journal of Concrete Structures and Materials

RESEARCH

Open Access

Numerical FE Modeling and Design Methods of CCES Columns with Normal-Weight Crushed Dolomite Coarse Aggregate Fully Embedded IPE Steel-Section

Mostafa M. A. Mostafa[1*]

Abstract

The composite concrete-encased steel (CCES) column member is made by the steel section embedded and covered in concrete from all sides. Due to the ability of the composite sections to bear heavy loads while using smaller sections, CCES columns have been widely used. Analytical studies on the CCES columns' behavior using crushed dolomite coarse aggregate (CDCA) with different shear connectors (SCs) types/shapes and sizes under axial loads are described here. This study also aims to evaluate the current design methods to determine the ultimate capacity of the CCES with CDCA concrete columns using nine available codes. The results show that the finite element (FE) analysis could accurately predict the ultimate capacity of the CCES columns; the column's capacity improved by about 41.75% as f_{cu} increased by 60%. Increasing the IPE-shaped steel strength (f_{ss}) strategy is not very effective and gives brittle behavior even though enhancing the f_{ss} improves the capacity. The column's capacity increased as the tie stirrups and steel bars ratios increased. The column's capacity increased by about 17.63%, as steel bars ratios increased by 155.49%. The efficiency factors increased slightly as tie stirrups were raised but slightly decreased as steel bar ratios increased. Using the SCs system increases the columns' capacity by an average value of about 4.9% of the specimen without SCs. The computed capacities using the nine available codes are conservative and safe. The closest estimates made by the YB9082-06 code are 26% less on average than the test results; in contrast, the safest predictions made by the ECP-LRFD code are 68% less, on average, than test results.

Keywords Steel-reinforced concrete (SRC), Composite concrete-encased steel (CCES), Shear connectors, FE analysis, Design codes, Dolomite coarse aggregate, Confinement

Journal information: ISSN 1976-0485 / eISSN 2234-1315.

*Correspondence:
Mostafa M. A. Mostafa
mostafa.mohamed@azhar.edu.eg
Full list of author information is available at the end of the article

Graphical Abstract

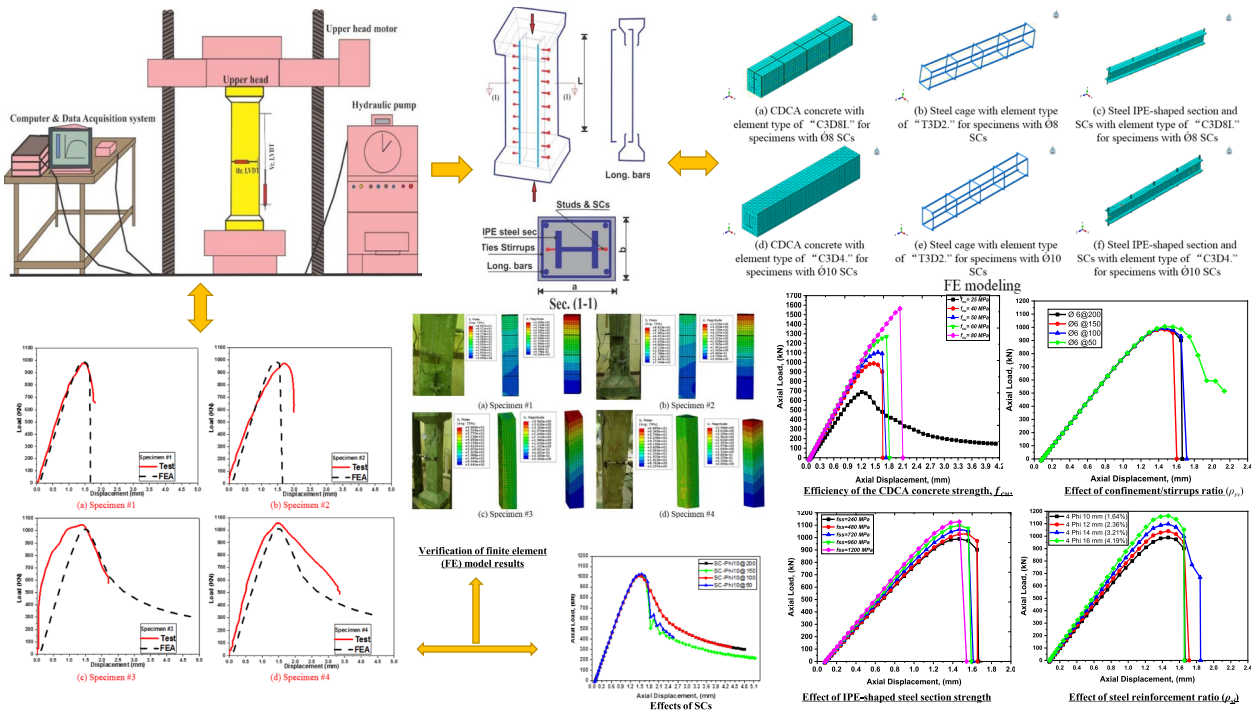

1 Introduction

The composite columns can be divided into two main types, which are composite concrete-filled steel tube (CFST) columns (Zhang et al., 2023) and composite concrete-encased steel (CCES) columns (Mostafa et al., 2019). The CCES column consists of a steel section embedded in reinforced concrete (RC); it is a widely used column due to its numerous advantages, including higher strength, ductility, and fire protection for the steel section; it also gives a smaller cross-section than the conventional column and reduces the amount of used concrete, thus improving the environment by reducing the harmful emissions from concrete production (Hui et al., 2020; Mostafa et al., 2019, 2022a). The design codes have different design methods for designing the CCES columns, which treat the composite column as a steel column strengthened with concrete or as an RC column maintained by special reinforcement. Besides, the capacity of the CCES columns is evaluated as the sum of the strengths of both components, concrete and steel reinforcements. The differences in the capacity predicted by existing codes are attributed to the differences in the philosophy of design, such as compatibility and strain. The discrepancy is due to the changes in allowable material properties, dimensions limits, and factors of safety (Soliman et al., 2013).

The confinement by increasing the ties number is a strengthening technique to improve the column's behavior. Shear connectors (SCs), made by welding studs or reinforcing bars to the encased steel section, can transfer the shear between the steel and concrete surfaces. The effects and use of SCs have been widely studied by many scholars worldwide, especially for members subjected to flexural or eccentric loads or to prevent slippage between concrete and steel in the load application zones (Alharthi et al., 2022; Chen et al., 2022; Sun et al., 2021; Xue et al., 2020a, 2020b; Yang & Li, 2020; Yang et al., 2019a, 2019b, 2021a, 2021b; Yu et al., 2020). A numerical investigation of the CCES columns with partially encased NWC at normal and high temperatures was also conducted (Štefan et al., 2019). Push-out tests and parametric analysis were used to numerically study the mechanical performance of a short steel channel-section SCs in a composite deck with a thin ultra-high performance concrete (UHPC) plate; when the SCs height increased from 50 to 80 mm, the shear strength improved, and the SCs arrangement orientation was a critical factor to the SCs' uplift resistance (Zhao et al., 2020). A study on the axial behavior of high-strength CCES columns without SCs,

including analytical modeling, considering confinement effects provided by tie stirrups and steel sections, has been done by Lai and Liew (2021). The behavior of ultra-high strength composite concrete-encased steel (USC-CES) columns subject to fire has been studied by Du et al. (2021). In addition, Venkateshwaran et al. (2021) studied the high-strength CCES column member by replacing traditional steel bar reinforcement with steel fibers, producing ductile structural behavior and shorter construction time and stopping the spread of microcracks by using the tiny straight steel fibers in their specimens. In order to estimate the N-M relationship, the authors proposed two analytical methods for specimens with and without traditional steel longitudinal bars reinforcement. They also studied the buckling behavior of CCES columns with hooked-end steel fibers (Venkateshwaran et al., 2022). According to Pereira1a et al. (2016), local buckling of the steel section occurs at 55% of the maximum load, resulting in unexpectedly low capacity and possibly related to the early flaws in the steel sections.

From the previous literature, it can be noted that most of the existing studies in the field of SCs were for elements under flexural loads or for composite slabs and beam systems. The current studies of the CCES columns with IPE-shaped steel sections and ties stirrups lack investigation of the influence of SCs under axial forces through FE analysis and analytical modeling; however, the behavior of the CCES columns under other types of loading has been studied using different parameters. For these reasons, the analytical analysis of the CCES columns under axial loads needs further investigation.

This paper numerically investigates the effects of different study parameters on the rectangular CCES columns using crushed dolomite coarse aggregate (CDCA) with fully embedded IPE steel sections under axial compressive loads using different SCs with different sizes and shapes and tie stirrups ratios, etc. First, on the basis of the constitutive material models for various components of the columns, stress–strain constitutive material models were developed to be input in the FEA model using ABAQUS software, including the CDCA concrete material and steel material, etc. The validity of the model was checked and compared to the test results conducted by the author (Mostafa, 2016) in terms of load–deformation curves and the ultimate capacities of the specimens. In this paper, analytical and theoretical calculations were also conducted using nine available codes (YB9082-06 (YB9082-06, 2007), CECS159 (CECS-230-, 2008, 2009), Hong Kong code (Code-11, 2011), ECP203 (ECP-203, 2018), ECP-LRFD (ECP-SC-LRFD, 2012), ACI318M (ACI318M-14, 2014), AISC-360-16, (2016), BS-5400-05 (BS.5400-5, 2002), and Eurocode-4 (Eurocode-4, 2004) to predict the ultimate axial capacities and to determine whether it would be feasible to apply these methods on CCES columns with CDCA concrete under axial load. The computed design codes results were compared with the experimental and FE results. Finally, parametric studies were conducted using the verified FE model regarding the influences of CDCA concrete strength, IPE-shaped section steel strength (f_{ss}), confinement/tie stirrups ratio (ρ_{sv}), SCs spacings and types, and the steel reinforcement ratio (ρ_{sl}) on the axial behavior of the columns.

2 Columns Finite Element (FE) Modeling

FE software, ABAQUS, was used to conduct the analysis. The specimens' column upper and lower heads were used in the experiments to distribute the load evenly and prevent CDCA concrete from crashing by the machine head in the experiments. However, these things are not found in the FE analysis modeling. In the FE analysis modeling, fixed-end boundary conditions for the lower whole cross-section and the rigid body constraint option were used to tie the loading reference point to the whole cross-section in the upper part. The following is a brief description of the experimental work used to verify the analytical studies.

2.1 Brief Description of the Experimental Work

A brief explanation of the CCES columns' experimental work exists here; more details about the experimentally studied column specimens are presented by Mostafa (2016). Column specimens with a rectangle cross-section of 120 mm × 160 mm and a total height of 1100 mm were prepared using crushed dolomite coarse aggregate (CDCA) with a maximum nominal size of 10 mm according to ES: 1109/2008 and tested under axial vertical compressive load with different shear connectors (SCs), with different spacing. The specimens have four longitudinal RFT bars with a diameter of 10 mm, horizontal ties with a diameter of 6 mm, and encased IPE.No.8 shaped steel section. They were used to verify the FE analysis results here. The actual concrete dimensions of the column specimens were 120 × 160 × 800 mm. The columns have concrete heads at the upper and lower ends with a cross-section of 260 mm × 300 mm. The height of the head was 150 mm, as shown in Fig. 1a. The heads were provided at the upper and lower ends of the column to distribute the load evenly and to prevent the premature crushing of CDCA concrete of the specimens by the machine heads. The used CDCA concrete strength grade (f_{cu}) was 40 MPa, which represents the actual measured CDCA concrete compressive strength value of 53.7 MPa for all columns (the grade was calculated based on the BS mix design method). To determine the actual CDCA concrete compressive strength and to quality control the concrete material

used in the test, six standard CDCA concrete cubes (150 × 150 × 150 mm) were made, three to be tested after seven days and the other three to be tested simultaneously by applying the test loads on the specimens. The embedded steel section type was IPE.No.8, which had a steel section ratio of 3.98%. Table 1 shows the properties and details of the tested column specimens used here. In the experimental test, two LVDTs were placed vertically and horizontally on the specimens' sides to capture the specimens' vertical and horizontal displacements, respectively. The measurement lengths in the vertical and horizontal directions were 640 mm and 130 mm, respectively. Strain gauges were used to record the strains of the IPE-shaped steel sections, reinforcement bars, and tie stirrups. Fig. 1b shows the general cross-section of the tested specimens.

2.2 Constitutive Material Model for CDCA Concrete, IPE-Shaped Steel Section, Vertical Longitudinal Reinforcement Bars, and Ties Stirrups

Different available models have been tried to represent the studied concrete in the analysis through sensitivity analysis performed to select an appropriate model; the Mander model (Mander et al., 1988a, 1988b) was found to be suitable and gave the closest results to the test, so it was used to model the CDCA concrete in ABAQUS software (see Fig. 2a). The linear and nonlinear material parts were captured. The type of elastic part is isotropic, which was simulated using Young's modulus and poisons ratio. The concrete damage plasticity model was used to model the plasticity of the CDCA concrete; the used Dilation Angle was equal to 30, the used Eccentricity value was equal to 0.1, the value of f_{b0}/f_{c0} was equal to 1.16, the value of the factor K was equal 0.6667, the Viscosity Parameter value was equal 0.001, the mass Density off the CDCA concrete was equal 2.5 g/cm^3. The Poisson's ratios for the CDCA concrete and steel were equal to 0.2 and 0.3, respectively, the density of the steel was equal to 7.85 g/cm^3, and the curve type was bilinear with ascending post-yield part. The used steel bars were according to ESS: 262 and ISO: 6935. High-grade steel bars of St. 40/60 and normal mild steel smooth bars St. 24/35 were used for longitudinal reinforcement and tie stirrups, respectively; the yield strength (f_y) and elasticity modulus (E_s) of steel longitudinal reinforcement were 400 MPa and 220000 MPa, respectively, the f_y and E_s of steel tie stirrups were 240 MPa and 200000 MPa, respectively. The yielding strength (f_{ss}) and E_s of encased rolled steel sections (IPE.No.8.) were 240 MPa and 200000 MPa, respectively. The type of elastic part was isotropic, while the type of hardening part was kinematic. The application method of kinematic hardening was done by selecting the type of hardening part as kinematic in the plastic material part, as there are different options in ABAQUS for the type of hardening part. Kinematic steel hardening

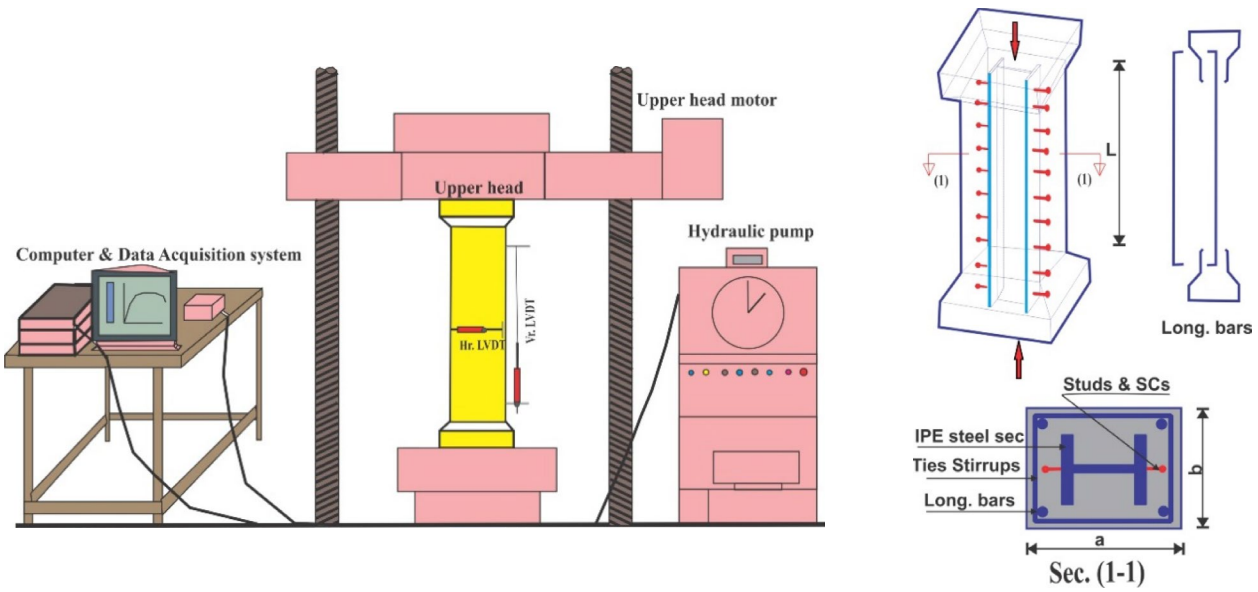

(a) Test setup and schematic diagram

(b) specimens geometry dimensions and steel reinforcement (units: mm)

Fig. 1 Test setup and specimens' details: (a) Test setup and schematic diagram; (b) specimens geometry dimensions and steel reinforcement (units: mm)

Table 1 Properties of tested CCES column

Specimen no.	Concrete dimensions b×a×L (mm^3)	f_{cu} *(MPa)*	Main RFT. (long. bars)	Ties φ6@S	Shear connectors (SCs)	IPE-shaped steel section	IPE steel section ratio ρ_a(%)	Reinforcement ratio ρ_{rs}(%)	Area of concrete $A_{c\ (net)}$ mm^2	Area of RFT A_{sc} mm^2	Area of steel sec A_{ss} mm^2
Specimen #1	120×160×800	40	4Ø10	φ6@200	Connector ø8@200	IPE.No.8	3.98	1.64	18436	314.16	764
Specimen #2	120×160×800	40	4Ø10	φ6@200	Connector ø8@100	IPE.No.8	3.98	1.64	18436	314.16	764
Specimen #3	120×160×800	40	4Ø10	φ6@200	Connector ø10@200	IPE.No.8	3.98	1.64	18436	314.16	764
Specimen #4	120×160×800	40	4Ø10	φ6@200	Connector ø10@100	IPE.No.8	3.98	1.64	18436	314.16	764

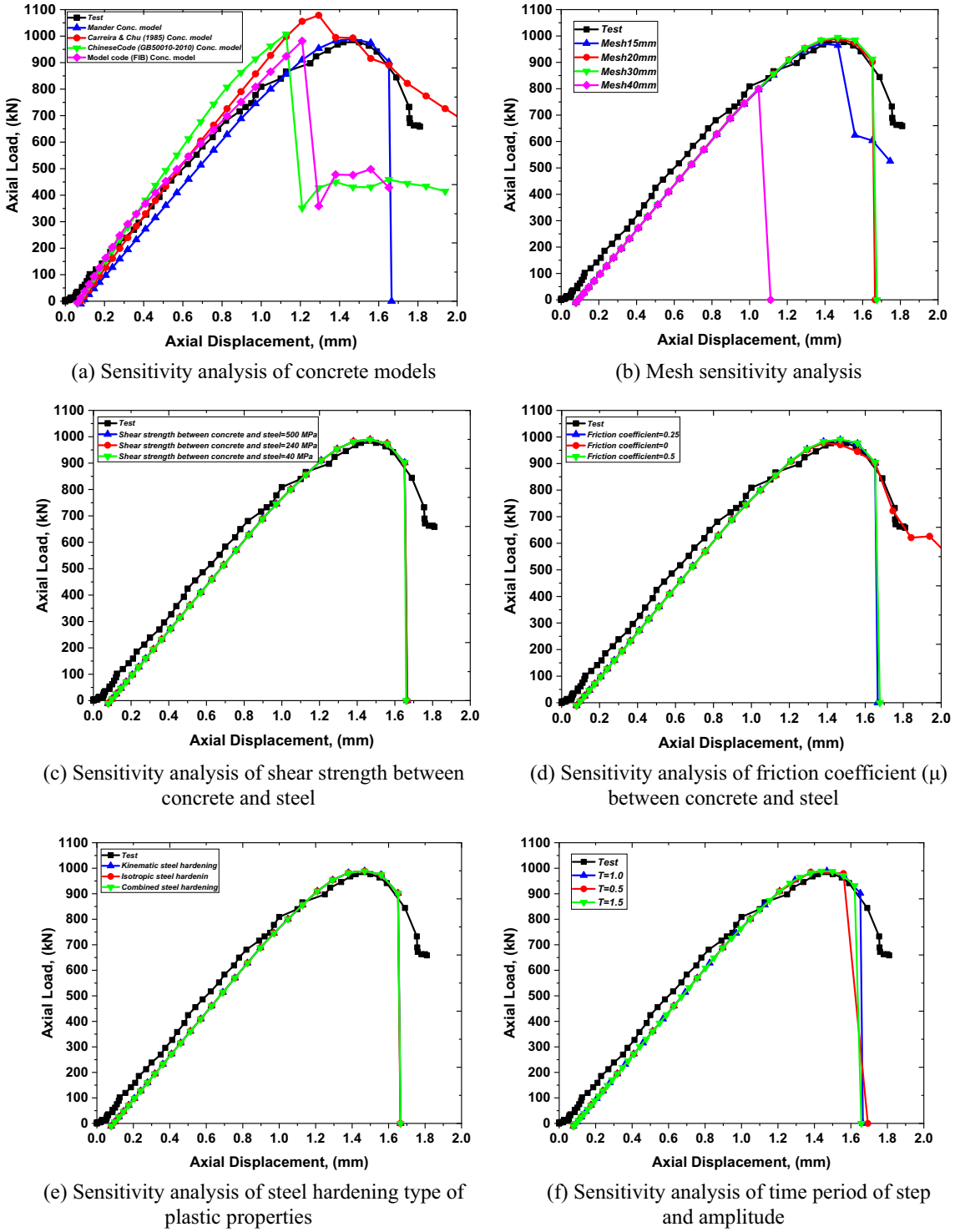

(a) Sensitivity analysis of concrete models

(b) Mesh sensitivity analysis

(c) Sensitivity analysis of shear strength between concrete and steel

(d) Sensitivity analysis of friction coefficient (μ) between concrete and steel

(e) Sensitivity analysis of steel hardening type of plastic properties

(f) Sensitivity analysis of time period of step and amplitude

Fig. 2 Sensitivity analysis studies: (a) Sensitivity analysis of concrete models; (b) Mesh sensitivity analysis; (c) Sensitivity analysis of shear strength between concrete and steel; (d) Sensitivity analysis of friction coefficient (μ) between concrete and steel; (e) Sensitivity analysis of steel hardening type of plastic properties; (f) Sensitivity analysis of time period of step and amplitude

was found to be suitable here and gave the nearest ultimate value to the test result (see Fig. 2e).

2.3 Elements Types and Mesh Sizes

The linear line type "T3D2" element type, using a linear 3D truss with a 2-node, was used for the steel ties and bars.

The linear hexahedron (Hex) type "C3D8I" element type, using eight nodes of linear brick and incompatible modes, for the CDCA concrete, IPE-shaped steel section, and steel SCs, were found to be suitable in meshing and simulating the first two specimens, specimens with Ø8 SCs. While the four-node tetrahedral (Tet) element "C3D4" element type with one integration point for the CDCA concrete, IPE-shaped steel section, and steel SCs were found to be suitable in meshing and simulating the second two specimens, specimens with Ø10 SCs. Fig. 3a-f shows the FE modeling and element types used in simulating the specimens. Based on mesh sensitivity analysis and to accurately simulate the axial behavior of the CCES columns with CDCA concrete, it was found that a 20 mm element size was suitable for all column element types (see Fig. 2b). Although the curve with 15 mm mesh sizes is near to the curve with 20 mm mesh sizes, the displacement at ultimate load (1.379 mm) had a large difference than the test (1.50 mm) and for 20 mm mesh sizes (1.469 mm). The mesh sizes smaller than these sizes showed longer time-consuming, aborted due to error of near nodes or due to the ratio of deformation speed to wave speed exceeding 1.0.

2.4 Interaction Between the Steel and CDCA Concrete in the FE Modeling

This section describes the interaction between the CDCA concrete and IPE-shaped steel section, steel longitudinal bars, tie stirrups, and SCs in the FE analysis modeling. The surface contact between the CDCA concrete and the IPE-shaped steel section or SCs of the CCES column members was general contact. If the bonding capacity is more significant than the applied stress throughout the test, the steel and CDCA concrete surfaces' cohesive bonding resists the bond stresses. Slippage in the surface occurs with the loads increasing and shear stresses beyond the bond capacity. Crack initiation and propagation happen, which is the reason for the uplift force on the used SCs when the normal stress overdoes the tension strength capacity of the surface (Lin et al., 2014). Cohesive contact interaction type "*CONTACT PAIR option" was applied to the surface between the CDCA concrete and IPE-shaped steel section to simulate the interaction between the CDCA concrete and steel in the ABAQUS; in this way, two surfaces should be defined. The first is the CDCA concrete surface surrounding the IPE-shaped structural steel section, and the second is the IPE-shaped structural steel section surface; the interface components are produced between the two surfaces to track the second surface's displacement with respect to the first one. The "Hard Contact Presser" was used for normal performance between CDCA concrete and IPE-shaped structural steel section, and "Penalty Fracture Formulation" with a friction factor (μ) equal to 0.25 (Ellobody et al., 2011) and specified shear stress limit equal to 500 MPa, was used for tangential performance

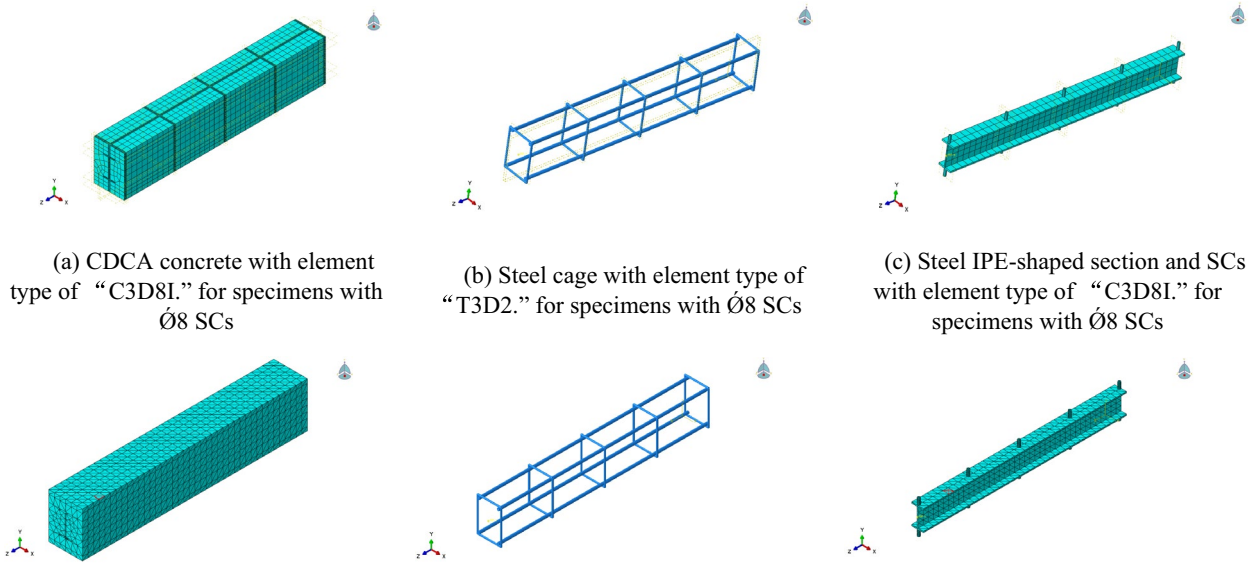

(a) CDCA concrete with element type of "C3D8I." for specimens with Ø8 SCs

(b) Steel cage with element type of "T3D2." for specimens with Ø8 SCs

(c) Steel IPE-shaped section and SCs with element type of "C3D8I." for specimens with Ø8 SCs

(d) CDCA concrete with element type of "C3D4." for specimens with Ø10 SCs

(e) Steel cage with element type of "T3D2." for specimens with Ø10 SCs

(f) Steel IPE-shaped section and SCs with element type of "C3D4." for specimens with Ø10 SCs

Fig. 3 FE modeling: (a) CDCA concrete with element type of "C3D8I." for specimens with Ø8 SCs; (b) Steel cage with element type of "T3D2." for specimens with Ø8 SCs; (c) Steel IPE-shaped section and SCs with element type of "C3D8I." for specimens with Ø8 SCs; (d) CDCA concrete with element type of "C3D4." for specimens with Ø10 SCs; (e) Steel cage with element type of "T3D2." for specimens with Ø10 SCs; (f) Steel IPE-shaped section and SCs with element type of "C3D4." for specimens with Ø10 SCs

based on the sensitivity analysis (see Fig. 2c); although the value of shear strength values between concrete and steel has shown a small effect, the value of 500 MPa was found to give the closest result to the test results with value of ultimate column's capacity of 989.036 kN in comparison to 989.074 kN and 989.208 kN for specimens with shear strength values between concrete and steel equal 240 MPa and 40 MPa, respectively. Also, the sensitivity analysis of friction coefficient (μ) between concrete and steel was done, as shown in Fig. 2d; the μ = 0.25 was found to be suitable and gave the closest result to test results, although the μ = 0 showed better curve, the displacement at ultimate load (1.379 mm) had a large difference than the test (1.50 mm) and for μ = 0.25 (1.469 mm). Using this property between CDCA concrete and IPE-shaped structural steel, when the two designated surfaces come into contact, the normal forces applied to the first surface can be transmitted between them. When the two specified surfaces separate, the relative movement between the two surfaces can still be observed, but normal forces to the first surface are not passed. In any case, the two designated surfaces cannot penetrate each other in this manner. The steel longitudinal and bars tie stirrups were assembled in the CDCA concrete as an "Embedded region" type.

2.5 Boundary Conditions

In the CCES column members, one reference point (RP) was modeled at the top of the specimens to be connected/tied to the top surface as a rigid body and then was used to apply the boundary conditions and loading through this point. The loads were applied in the upper reference point as a dynamic explicit step since the static general step requires too much time to solve the model, and results are usually aborted because of convergence reasons since the usage of a dynamic explicit with CDP model produced accurate forecasts of the capacity (Begum et al., 2013; Mostafa et al., 2021). The lower surface of the specimens was fixed. Similar to Lai et al., (2019a), the load gradually increased by raising the displacement utilizing the displacement control method (to displace in the vertical direction, -U3) in a smooth step amplitude-type manner, as it was done by Sun et al., (2019). The time period equal to 1.0 was found to be suitable in the used explicit solver after trying different values (see Fig. 2f), the modeling approach took into account the nonlinear geometry, and the force was applied incrementally (Ellobody & Young, 2011).

2.6 The Defects from Initial Imperfections and Residual Stresses

The initial imperfection and residual stress were considered to take any manufacturing defect during and/or after the industry stage of steel sections due to uneven cooling or small bending/buckling of the steel section. The initial imperfection using critical eigenvalue buckling modes was used. The residual stress was considered through predefined field stress available in ABAQUS, and direct specification was utilized. To simulate the compressive behaviors of engineered cementitious composites-concrete encased steel columns with compact steel sections, a 3D nonlinear FE model was created by Khan et al. (2020); their suggested FE model included contact interactions, material and geometric nonlinearities, and geometric imperfections to produce accurate predictions. The FEA predictions showed better agreement with test results when the initial imperfections were taken into consideration (Khan et al., 2020; Lai et al., 2019a, 2019b; Pereira1a et al., 2016). The initial imperfection effect and the residual stresses effect in the IPE-shaped steel section were taken into account in the analysis. Three buckling modes (eigenmode 1, 2, and 3) were used in the analysis. The buckling mode obtained by the ABAQUS Eigenvalue analysis is normalized to unity 1.0, and the buckling modes were factored by multiplying it by the initial overall geometric imperfection magnitude. Following the ABAQUS eigenvalue prediction, the factored initial imperfection buckling mode was imported into the nonlinear load–displacement analysis.

3 Verification of Finite Element (FE) Model Results

Table 2 and Fig. 4a-d plot and list the comparison of FEA modeling to test results. Also, Fig. 5a-d shows the failure mode and deformation comparison between the test and FE results of the CCES column member at the ultimate capacity. The resulting contour is not symmetrical due to the initial imperfection that was taken into account to capture the real field column and to consider any manufacturing defect during and/or after the industry stage. The two specimens with shear connectors of Ø10 exhibited a ductile behavior, while the other two specimens with shear connectors of Ø8 exhibited a brittle behavior; this upgraded behavior for the two specimens with shear connectors of Ø10 may be attributed to the fact that the specimens with shear connectors of Ø10 improved the interaction and bond between the concrete and ribbed high-strength steel shear connectors rather than the smooth mild steel shear connectors for the other two specimens with shear connectors of Ø8. Generally, the FEA analysis results agree reasonably with the test results that validate the numerical model efficiency. The average axial load ratio value of the test to numerical results ($P_{u,Test}/P_{u,FE}$) of 1.019 and a coefficient of variation of 0.031 are observed here. The average axial displacement ratio value of the test to numerical results ($\Delta_{u,Test}/\Delta_{u,FE}$) of 1.036 and a coefficient of variation of 0.082 are also observed here. The predictions are averagely conservative and safe.

Table 2 Comparison of the ultimate capacity

Specimen no.	$P_{u,Test}$, (kN)	$P_{u,FE}$, (kN)	$P_{u,Test}/P_{u,FE}$	$\Delta_{u,Test}$, (mm)	$\Delta_{u,FE}$, (mm)	$\Delta_{u,Test}/\Delta_{u,FE}$
Specimen #1	976.860	989.036	0.988	1.500	1.469	1.021
Specimen #2	980.660	985.383	0.995	1.696	1.469	1.155
Specimen #3	1056.420	1010.840	1.045	1.400	1.469	0.953
Specimen #4	1056.420	1009.730	1.046	1.491	1.468	1.015
Mean	1017.590	998.747	1.019	1.522	1.469	1.036
SD			0.031			0.085
COV			0.031			0.082

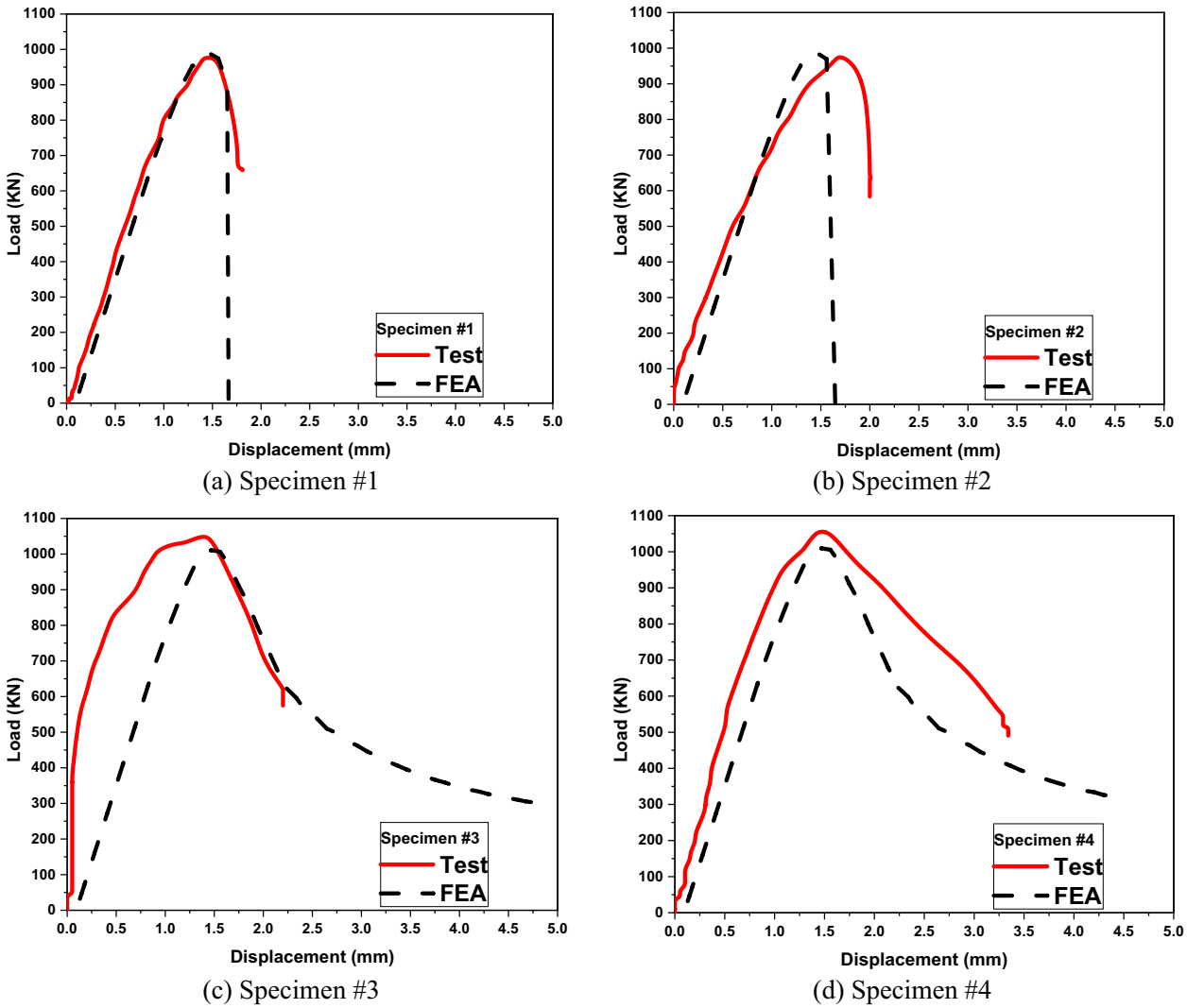

Fig. 4 Comparison of FEA modeling to test results: (a) Specimen #1; (b) Specimen #2; (c) Specimen #3; (d) Specimen #4

4 Parametric Study

Progress has been made in understanding how shear connectors (SCs) between concrete and steel and other parameters affect beams and slabs over the past years. Still, less is known about how the SCs and other factors affect the behavior of CCES columns with CDCA, especially under axial loads. The studied parameters that affect the axial capacity of the CCES columns with

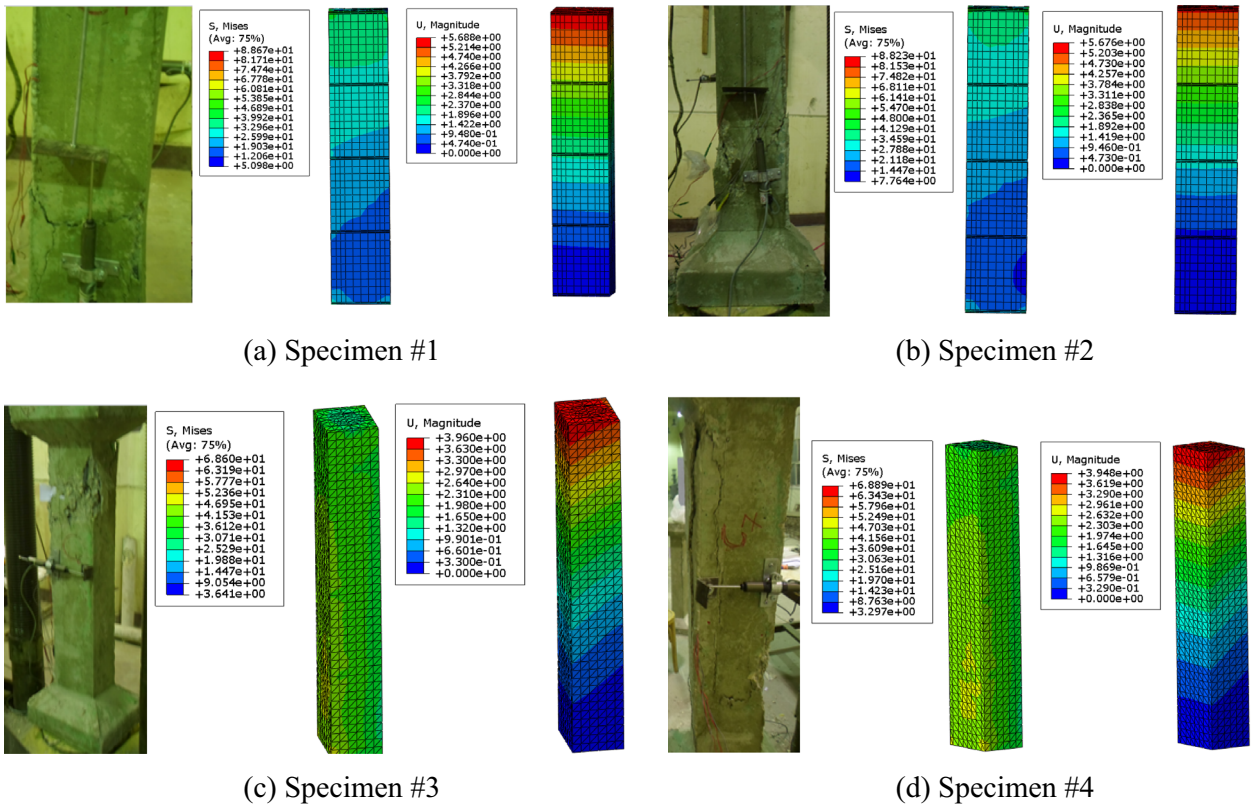

Fig. 5 Failure mode comparison and deformation of CCES column member at the ultimate capacity: (a) Specimen #1; (b) Specimen #2; (c) Specimen #3; (d) Specimen #4

CDCA and IPE-shaped steel sections are presented here. The studied influencing parameters reported here were investigated by changing these factors with the constant of the other factors. The following four factors were chosen to be the main parameters for the analysis in this paper through the analytical finite element (FE) studies: the impact of SCs, with different SCs with different types/shapes and sizes to provide slip interface resistance between IPE-shaped steel and CDCA concrete, the impact of confinement by tie stirrups, the impact of CDCA strength, the impact of steel longitudinal bars ratio, and the impact of IPE-shaped steel strength. Table 3 demonstrates the range of the studied parameter factors. Table 4 displays the effects of different parameters on the analysis results of the ultimate capacity of the CCES columns with CDCA concrete. Generally, for all the specimens, the curves presented in different sub-sections show that the loads increase gradually with increasing deformation till reaching the ultimate axial load capacity, then start to decrease with increasing displacements.

4.1 The Effect of CDCA Concrete Strength

The effect of concrete strength has been studied by many scholars before (Du et al., 2021; Venkateshwaran et al.,

Table 3 The ranges of the studied parameters

The studied columns' cross-section dimensions $b \times t \times L$ (mm × mm × mm)	**120 × 160 × 800**
IPE-shaped steel section	IPE.No.8
IPE-shaped steel section strength, f_{ss}*(MPa)*	240, 480, 720, 960, and 1200
CDCA concrete strength, f_{cu}*(MPa)*	25, 40, 50, 60, and 80
Tie stirrups spacings *(Tie* stirrups *ratio %)*	@200 (0.59%), @150 (0.78%), @100 (1.18%), and @50 (2.36%)
Shear connectors (SCs) spacings	Ø8 and Ø10 (@200, @150, @100, and @50)
SCs types	Bars SCs and studs SCs
Longitudinal steel reinforcement ratio (ρ_{sl})	Longitudinal RFT bars 4Φ10 (1.64%), 4Φ12 (2.36%), 4Φ14 (3.21%), and 4Φ16 (4.19%)

2021). The capacity of the investigated columns is heavily influenced by the strength of the concrete. Using the validated model, Fig. 6 and Table 5 depict the effect of CDCA concrete strength (f_{cu}) on the columns' capacities (P_u) and overall behaviors of the columns, demonstrating that as CDCA concrete strength increased, the ultimate axial compression capacities increased for the tie stirrup spacing and other parameters are not changed. A maximum of 80 MPa of f_{cu} was used. Table 5 displays the percentage outcomes as well as the effectiveness of increasing the f_{cu}. The results reveal that the P_u increases with the increase of f_{cu}. For example, the P_u of the specimen with $f_{cu}=40$ MPa improved by about 41.75% compared to the specimen with the smallest concrete strength, $f_{cu}=25$ MPa, despite a 60% increase in the used f_{cu}.

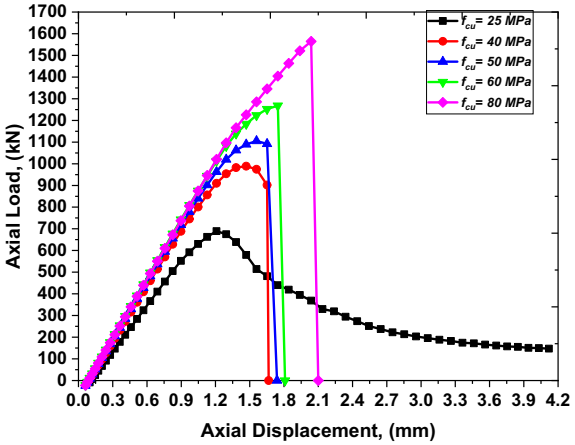

Fig. 6 Efficiency of the CDCA concrete strength

Table 4 The effects of different parameters on the analysis results of the ultimate behaviors

Parameters	CDCA concrete strength, MPa	IPE-shaped steel strength, f_{ss} (MPa)	Steel long. bars (ratio, ρ_{sl} %)	Confinement/ tie stirrups spacings, @ mm	Tie stirrups ratio, ρ_{sv} %	Shear connectors (SCs), @ mm	Ultimate axial capacity, $P_{u,FE}$, (kN)	Ultimate displacement Δ_u, (mm)
Effect of steel strength	40	240	4Φ10 (1.64%)	φ6@200	0.59	SCØ8@200	989.04	1.47
	40	480	4Φ10 (1.64%)	φ6@200	0.59	SCØ8@200	1028.32	1.47
	40	720	4Φ10 (1.64%)	φ6@200	0.59	SCØ8@200	1064.77	1.47
	40	960	4Φ10 (1.64%)	φ6@200	0.59	SCØ8@200	1097.80	1.47
	40	1200	4Φ10 (1.64%)	φ6@200	0.59	SCØ8@200	1127.81	1.47
Effect of CDCA concrete strength	25	240	4Φ10 (1.64%)	φ6@200	0.59	SCØ8@200	689.16	1.21
	40	240	4Φ10 (1.64%)	φ6@200	0.59	SCØ8@200	989.04	1.47
	50	240	4Φ10 (1.64%)	φ6@200	0.59	SCØ8@200	1105.07	1.56
	60	240	4Φ10 (1.64%)	φ6@200	0.59	SCØ8@200	1268.25	1.74
	80	240	4Φ10 (1.64%)	φ6@200	0.59	SCØ8@200	1564.49	2.04
Effect of confinement/tie stirrups ratio	40	240	4Φ10 (1.64%)	Ø6 @200	0.59	SCØ8@200	989.036	1.47
	40	240	4Φ10 (1.64%)	Ø6 @150	0.78	SCØ8@200	983.13	1.47
	40	240	4Φ10 (1.64%)	Ø6 @100	1.18	SCØ8@200	991.545	1.47
	40	240	4Φ10 (1.64%)	Ø6 @50	2.36	SCØ8@200	1006.42	1.47
Effect of SCs spacings and types	40	240	4Φ10 (1.64%)	φ6@200	0.59	SCØ8@200	989.04	1.47
	40	240	4Φ10 (1.64%)	φ6@200	0.59	SCØ8@150	987.63	1.47
	40	240	4Φ10 (1.64%)	φ6@200	0.59	SCØ8@100	985.38	1.47
	40	240	4Φ10 (1.64%)	φ6@200	0.59	SCØ8@50	991.13	1.47
	40	240	4Φ10 (1.64%)	φ6@200	0.59	SCØ10@200	1010.84	1.47
	40	240	4Φ10 (1.64%)	φ6@200	0.59	SCØ10@150	1016.703	1.559
	40	240	4Φ10 (1.64%)	φ6@200	0.59	SCØ10@100	1009.73	1.468
	40	240	4Φ10 (1.64%)	φ6@200	0.59	SCØ10@50	1027.806	1.559
	40	240	4Φ10 (1.64%)	φ6@200	0.59	studØ10@200	982.103	1.47
	40	240	4Φ10 (1.64%)	φ6@200	0.59	studØ10@150	978.66	1.47
	40	240	4Φ10 (1.64%)	φ6@200	0.59	studØ10@100	977.584	1.47
	40	240	4Φ10 (1.64%)	φ6@200	0.59	stud Ø10@50	999.34	1.47
Effect of steel reinforcement ratio	40	240	4Φ10 (1.64%)	φ6@200	0.59	SCØ8@200	989.04	1.47
	40	240	4Φ12 (2.36%)	φ6@200	0.59	SCØ8@200	1040.92	1.468
	40	240	4Φ14 (3.21%)	φ6@200	0.59	SCØ8@200	1098.35	1.468
	40	240	4Φ16 (4.19%)	φ6@200	0.59	SCØ8@200	1163.37	1.468

Table 5 Efficiency of the CDCA concrete strength

(MPa)	Capacity, P_u (kN)	Increasing of capacity, $+P_u$%	Increasing CDCA concrete strength, $+f_{cu}$%	$+P_u$%/$+f_{cu}$%
25	689.16	–	–	–
40	976.86	41.75	60	0.70
50	1105.07	60.35	100	0.60
60	1268.25	84.03	140	0.60
80	1564.49	127.01	220	0.58

The average efficiency factor of almost 62% indicates that this is a good strategy for raising the P_u of this kind of specimen, especially considering the cost of raising the f_{cu}. As displayed in Fig. 6, the strength–deformation relationships allow for analyzing the specimens' failure mechanisms. The peak point on the curve rises when the f_{cu} is increased. Although this is a less-than-ideal outcome from the construction perspective, the post-ultimate behaviors of the studied specimens with f_{cu} greater than 50 MPa show a rapid decline in the strength capacity, indicating occurrences of brittle collapses. This may be attributed to the sudden CDCA concrete cracking and potentially severe shattering with the greater applied force. The specimen with f_{cu} = 25 MPa gives ductile preferred and encouraging results than the other specimens. Based on the relations in Fig. 6, the trend appears more protuberant as f_{cu} increases, which points to a potential study point that should be studied in the future, particularly for specimens with a f_{cu} value greater than 50 MPa.

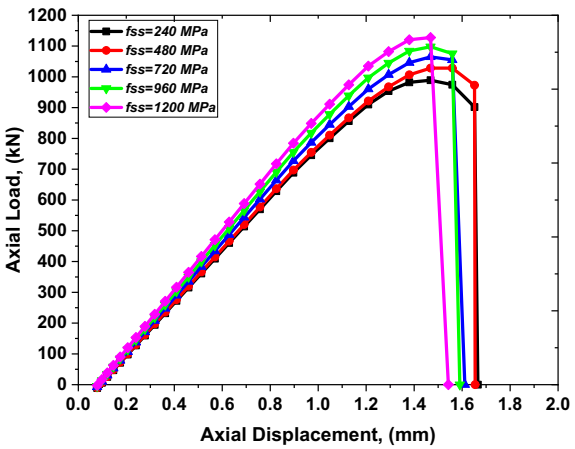

Fig. 7 Effect of IPE-shaped steel section strength

4.2 The Effect of IPE-Shaped Steel Strength (f_{ss})

The lightweight, high strength, cost-effectiveness, and other structural benefits of the structural element with high-strength steel are only a few of its advantages over other construction materials (Li & Cai, 2019). Using the verified model, Fig. 7 and Table 6 illustrate the impact of f_{ss} on the overall performance and the column members' ultimate strength capacity (P_u). The five specimens were selected to investigate the impact of raising the yield strength of the IPE-shaped steel section in the column members. The f_{ss} was raised from 240 to 1200 MPa.

As demonstrated in Table 6, P_u growth is relatively small compared to the growth in the f_{ss}. This increase results in a 3.97%, 7.66%, 11.00%, and 14.03% improvement in the P_u through the specimens with f_{ss} = 480, 720, 960, and 1200 MPa. Table 6 displays the effectiveness of f_{ss}; based on the pattern presented in the table, it can be concluded that as f_{ss} was raised, the efficiency factors decreased. This demonstrates that this strategy is not very effective, even though enhancing the f_{ss} improves the specimens' capacity. The relationships in Fig. 7 are used to point to the failure of the specimens that have been subjected to the influence of changing the f_{ss}. As the f_{ss} value increased, the specimens' behavior became more brittle; this is attributed to the increasing carbon percentage as the steel strength grade increased, which increased the stiffness and decreased the elongation deformability of steel. These are not preferred or encouraging results as was found in the specimens with f_{cu} higher than 50 MPa that show brittle failure mode in the analyzed specimens for the effect of the f_{cu}.

4.3 Effects of Confinement/Tie Stirrups Ratio (ρ_{sv})

Most research and codes neglect the confinement effects and the shear connectors (SCs) (Soliman et al., 2013) on the capacity of the column elements. The confinement has a considerable impact on how the members behave when subjected to various sorts of loads (Berke & Massart, 2018; Mostafa et al., 2019; Tunc et al., 2021). Fig. 8 shows the impact of ρ_{sv} on the column's behavior; it also shows a similar pattern to the samples of the f_{ss} effect. The utilized amount of ρ_{sv} was changed from 0.59 to 2.36%, equivalent to corresponding tie stirrup spacings values of 200 mm to 50 mm of tie stirrups spacings. According to the results, as the ρ_{sv} was raised, the column's capacity also generally increased; for example, when the ρ_{sv}

Table 6 Efficiency of IPE-shaped steel section strength

Steel yield strength, f_{ss} (MPa)	Axial capacity P_u (kN)	Increasing of axial capacity ($+P_u$%)	Increasing steel yield strength ($+f_{ss}$%)	($+P_u$%)/($+f_{ss}$%)
240	989.04	–	–	–
480	1028.32	3.97	100.00	0.040
720	1064.77	7.66	200.00	0.038
960	1097.80	11.00	300.00	0.037
1200	1127.81	14.03	400.00	0.035

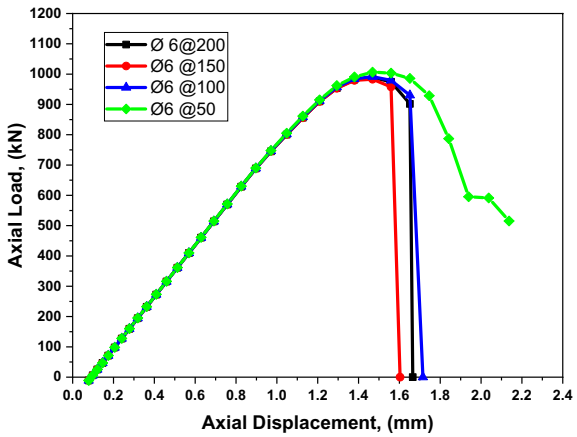

Fig. 8 Effect of confinement/tie stirrups ratio (ρ_{sv})

was raised from 0.59 to 2.36% by about 300%, the column's capacity slightly increased by about 1.76%. This was caused by the tie stirrups' confinement effects on the column specimens' CDCA concrete core and IPE-shaped steel section.

Table 7 shows that increasing horizontal ties generally increased the studied CCES columns' capacity under axial load. P_u growth is relatively inefficient compared to the growth in the ρ_{sv}. However, this increase only results in a 1.76% improvement in the P_u through the specimens. Based on the pattern presented in the table, the effectiveness of ρ_{sv} is that: As ρ_{sv} was raised, the efficiency factors slightly increased. This demonstrates that this strategy is useless even though enhancing the ρ_{sv} improves the specimens' capacity and post-ultimate ductility, especially for specimens with smaller tie stirrups spacings (@ 50 mm), as shown in Fig. 8. The bearing capacity and ductility slightly decreasing when the confinement ratio increased for the specimen Ø6 @ 150 may be attributed to the congestion of steel by increasing the steel ratio in the element, which causes easy cracking and separation between concrete and steel tie stirrups while improving the ρ_{sv} enhanced the specimens' capacity for specimens with smaller tie stirrups spacings (Ø6 @ 100 and Ø6 @ 50) and largely enhanced the specimen's post-ultimate ductility for the specimen (Ø6 @ 50) this may be attributed to that by decreasing the spacing between tie stirrups more, the concrete between steel decreased, and the crashed zone decreased so the bearing capacity and ductility controlled more by the large tie stirrups congestion rather than easy cracking and separation between concrete and steel tie stirrups. More studies need to be done to know more about the behavior of this type of column, and the ρ_{sv} factor in the CDMA structure with SCs needs to be set as a test variable in future research.

4.4 The Effect of Shear Connectors (SCs) Spacings and Types

The effect and use of shear connectors (SCs) have been widely used and studied by many scholars, especially for members under flexural or eccentric loads or to prevent the slippage between concrete and steel in the beam–column connection and/ or slab-to-steel girder zones (Alharthi et al., 2022; Chen et al., 2022; Han et al., 2017; Liu et al., 2018; Sun et al., 2021; Tunc et al., 2021; Xue

Table 7 Efficiency of the confinement/tie stirrups ratio (ρsv)

Confinement/tie stirrups spacings, mm	Tie stirrups ratio, ρ_{sv} %	Capacity, P_u (kN)	Increasing of capacity, $+P_u$%	Increasing tie stirrups ratio, $+\rho_{sv}$ %	$+P_u$%/$+\rho_{sv}$ %
Ø6 @ 200	0.59	989.036	–	–	
Ø6 @ 150	0.78	983.13	– 0.60	32.20	– 0.019
Ø6 @ 100	1.18	991.545	0.25	100.00	0.003
Ø6 @ 50	2.36	1006.42	1.76	300.00	0.006

et al., 2020a, 2020b; Yang & Li, 2020; Yang et al., 2019a, 2019b, 2021a, 2021b; Yu et al., 2020). The studs SCs significantly affect the new type of SRC columns under push-out loads due to improving the bond-slip behavior (Han et al., 2017; Mostafa et al., 2022b). Still, less is known about how SCs affect the column's behavior under axial loads. Fig. 9a-c and Table 8 show the effect of SCs spacings and types on the studied CCES column members' behavior. From the results, it can be shown that increasing the SCs spacings for the specimens with SCØ8 improves the capacity by about 0.21% for the specimen SCØ8@50 compared to specimen SCØ8@200, but the capacity for the other two specimens decreased. Also, increasing the SCs spacings for the specimens with SCØ10 improves the capacity by about 0.58% and 1.68% for specimens SCØ10@150 and SCØ10@50, respectively, compared to specimen SCØ10@200, but the capacity for the other specimen (SCØ10@100) decreased. Increasing the studs spacings for the specimens with studØ10 improves the capacity by about 1.76% for specimen studØ10@50 compared to specimen studØ10@200, but the capacity for the other two specimens decreased. It can be concluded that the SCs type SCs spacings effects are insignificant in columns under axial load.

As can be seen in Table 8, in comparison with specimen without connectors, using the SCs system technique made from steel reinforcement bars and stud SCs, with head and shank, welded to a flange of steel shape encased CDCA concrete increases the columns' capacity by an average value of about 4.9% of the control specimen without SCs. The columns' capacity increased by average values of 4.06%, 7.00%, and 3.65% for the series of specimens SCØ8, SCØ10, and studØ10, respectively.

4.5 The Effect of Longitudinal Steel Reinforcement Ratio (ρ_{sl})

Fig. 10 displays the impact of ρ_{sl} on the column's behavior; it also shows a similar pattern to the samples of the f_{cu} effect. The used amount of ρ_{sl} was changed from 1.64 to 4.19%, equivalent to corresponding steel reinforcement bars of 4Φ10 mm to 4Φ16 mm for each column. According to the results, as the ρ_{sl} was raised, the column's capacity also increased; for example, when the ρ_{sl} was raised from 1.64 to 4.19% by about 155.49%, the column's capacity increased by about 17.63%. This was caused by the effects of the larger value of steel ratio participating in bearing the load of the column specimens.

Table 9 shows that increasing ρ_{sl} generally increases the studied CCES columns' capacity under axial load. P_u growth is smaller compared to the growth in the ρ_{sl}. However, this increase results in a 17.63% improvement in the P_u through the specimens. Based on the pattern presented in the table, the effectiveness of ρ_{sl} is that: As

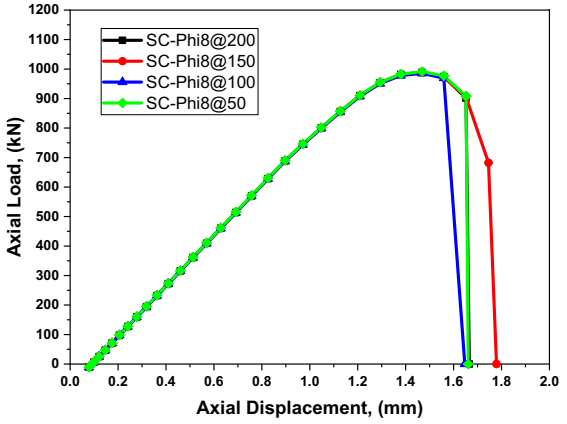

(a) SC-Phi8@S

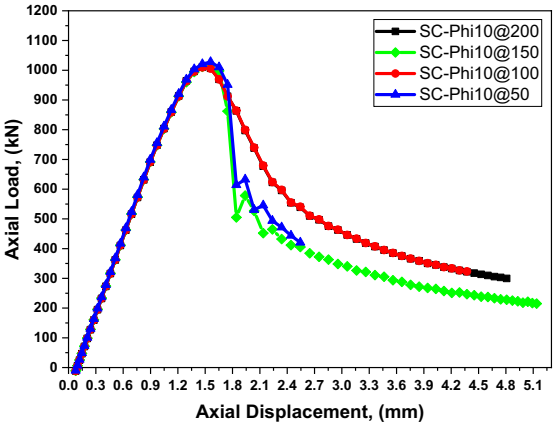

(b) SC-Phi10@S

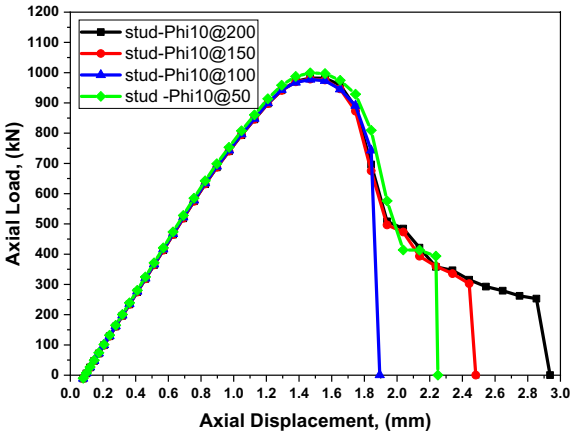

(c) Stud-Phi10@S

Fig. 9 Effects of SCs spacings and types: (a) SC-Phi8@S; (b) SC-Phi10@S; (c) Stud-Phi10@S

ρ_{sl} was raised, the efficiency factors slightly decreased, and the average efficiency factor was almost 12%. This result demonstrates that this strategy is not the best, especially considering the cost of raising the ρ_{sl}, even

Table 8 Effects of SCs spacings and types

SCs/stud type		SCs' spacings, mm	Capacity, P_u (kN)	In comparison with the first specimen with connectors			In comparison with a specimen without connectors		
				Increasing of capacity, $+P_u$%	Decrease in SC spacings, $+S$ %	$+P_u$%/$+S$%	Increasing of capacity, +Pu%	Decrease in SC spacings, $+S$ %	$+Pu$%/$+S$%
None	–	–	949.77	–	–	–	–	–	–
SCØ8	SCØ8@200	200	989.04	–	–	–	4.13	–	–
	SCØ8@150	150	987.63	– 0.14	– 25.00	0.006	3.99	– 25.00	– 0.159
	SCØ8@100	100	985.38	– 0.37	– 50.00	0.007	3.75	– 50.00	– 0.075
	SCØ8@50	50	991.13	0.21	– 75.00	– 0.003	4.35	– 75.00	– 0.058
SCØ10	SCØ10@200	200	1010.84	–	–	–	6.43	–	–
	SCØ10@150	150	1016.703	0.58	– 25.00	– 0.023	7.05	– 25.00	– 0.282
	SCØ10@100	100	1009.73	– 0.11	– 50.00	0.002	6.31	– 50.00	– 0.126
	SCØ10@50	50	1027.806	1.68	– 75.00	– 0.022	8.22	– 75.00	– 0.110
studØ10	studØ10@200	200	982.103	–	–	–	3.40	–	–
	studØ10@150	150	978.66	– 0.35	– 25.00	0.014	3.04	– 25.00	– 0.122
	studØ10@100	100	977.584	– 0.46	– 50.00	0.009	2.93	– 50.00	– 0.059
	stud Ø10@50	50	999.34	1.76	– 75.00	– 0.023	5.22	– 75.00	– 0.070

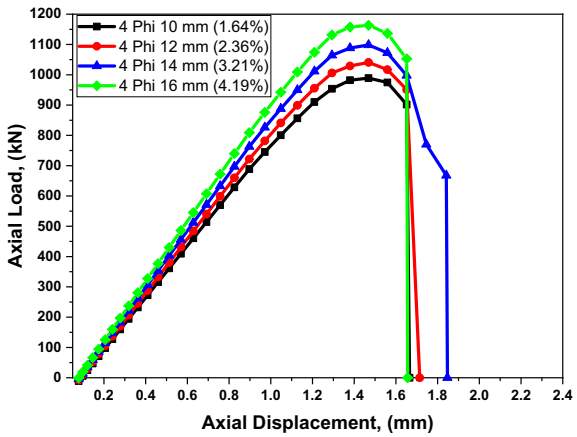

Fig. 10 Effect of steel reinforcement ratio (ρ_{sl})

though enhancing the ρ_{sl} improves the specimens' capacity. In addition, the post-ultimate ductility decreases for the specimen with ρ_{sl} larger than 3.21 (4Φ14 mm), as shown in Fig. 10.

5 Codes Theoretical Calculation

The design formulas of nine available codes of design (ACI318M-14, 2014; AISC-360-16, 2016; BS.5400-5, 2002; CECS-230-2008, 2009; Code-11, 2011; ECP-203, 2018; ECP-SC-LRFD, 2012; Eurocode-4, 2004; YB9082-06, 2007) were used to predict the ultimate capacity of the columns using the traditional methods presented in these codes for columns and to determine whether it would be feasible to apply these methods to CCES columns with CDCA concrete under axial load. The nine used available codes are YB9082-06 (YB9082-06, 2007), CECS159 (CECS-230-2008, 2009), Hong Kong code (Code-11, 2011), ECP203(ECP-203, 2018), ECP-LRFD (ECP-SC-LRFD, 2012), ACI318M (ACI318M-14, 2014), AISC-360-16, (2016), BS-5400–05 (BS.5400-5, 2002), and Eurocode-4 (Eurocode-4, 2004). The material properties used here, such as concrete strength, etc., were picked as stated in the code's provisions and their equations. The impact of the column's slenderness ratio is taken into account in the design calculations for the ultimate capacity used in AISC, (2016) and Eurocode-4, (2004). Table 10 displays the computed capacities using the nine available

Table 9 Efficiency of the steel reinforcement ratio (ρsl)

Long. bars	Long. bars ratio, ρ_{sl} %	Capacity, P_u (kN)	Increasing of capacity, $+P_u$%	Increasing of long. bars ratio, $+\rho_{sl}$ %	$+P_u$%/$+\rho_{sl}$ %
4Φ10 mm	1.64	989.04	–	–	–
4Φ12 mm	2.36	1040.92	5.25	43.90	0.119
4Φ14 mm	3.21	1098.35	11.05	95.73	0.115
4Φ16 mm	4.19	1163.37	17.63	155.49	0.113

Table 10 The ultimate axial capacity of the CCES columns with CDCA concrete according to the test result (Put) and nine available codes (Puo)

Code	Test result	FE result	YB9082-06 (YB9082-06, 2007)	CECS159 (CECS-230-, 2008, 2009)	Hong Kong code (Code-11, 2011)	ECP203(ECP-203, 2018)	ECP-LRFD (ECP-SC-LRFD, 2012)	ACI318M (ACI318M-14, 2014)	AISC-360-16, (2016)	BS-5400–05 (BS-5400-5, 2002)	Eurocode-4 (Eurocode-4, 2004)
Specimen number	$P_{ut,Test}$ (kN)	$P_{u,FE}$, (kN)	$P_{uo,YB}$ (kN)	$P_{uo,CECS}$ (kN)	$P_{uo,Hong\ Kong}$ (kN)	$P_{uo,ECP203}$ (kN)	$P_{uo,ECP\text{-}LRFD}$(kN)	$P_{uo,ACI}$ (kN)	$P_{uo,AISC}$ (kN)	$P_{uo,BS}$ (kN)	$P_{uo,EC4}$ (kN)
Specimen #1	976.86	989.04	809.4	701.7	624.3	735.7	607.1	695.1	699.3	612.8	797.4
Specimen #2	980.66	985.38	809.4	701.7	624.3	735.7	607.1	695.1	699.3	612.8	797.4
Specimen #3	1056.42	1010.84	809.4	701.7	624.3	735.7	607.1	695.1	699.3	612.8	797.4
Specimen #4	1056.42	1009.73	809.4	701.7	624.3	735.7	607.1	695.1	699.3	612.8	797.4

codes, and Table 11 compares them to the test and FE findings.

All the results of design codes give $P_{ut,Test}/P_{uo,codes}$ and $P_{ut,FE}/P_{uo,codes}$ larger than 1.0; this means that the determined capacities using these nine codes are conservative. The Chinese code, YB9082-06 (YB9082-06, 2007), provides the closest calculated ultimate capacity of the columns to both the test and FE results by average values of $P_{ut,Test}/P_{uo,YB}$ and $P_{u,FE}/P_{uo,YB}$ equal about 1.26 and 1.23, respectively, and the average values of coefficient of variation for both $P_{ut,Test}/P_{uo,YB}$ and $P_{u,FE}/P_{uo,YB}$ equal about 0.038 and 0.012, respectively. Moreover, the findings produced by the Egyptian code of steel, ECP-LRFD (ECP-SC-LRFD, 2012), are the most conservative. The average ratio of $P_{ut,Test}/P_{uo,ECP\text{-}LRFD}$ and $P_{u,FE}/P_{uo,ECP\text{-}LRFD}$ are 1.68 and 1.65, respectively; the coefficient of variation for $P_{ut,Test}/P_{uo,ECP\text{-}LRFD}$ and $P_{u,FE}/P_{uo,ECP\text{-}LRFD}$ are 0.038 and 0.012, respectively.

Finally, it can be said that the experimental/FE results and comparative studies demonstrate that, generally speaking, the anticipated results are less than the test and FE results, indicating that the computed columns capacities derived by the codes are practically on the safe side. The closest estimates made by YB9082-06 (YB9082-06, 2007) are 26% and 23% less, on average, than the test and FE results, respectively, while the safest prediction made by ECP-LRFD (ECP-SC-LRFD, 2012) are 68% and 65% less, on average, than the test and FE results, respectively (see Table 11).

6 Conclusions

Using the finite element (FE) analysis ABAQUS method, this paper numerically investigates the effects of different study parameters on the rectangular CCES columns using crushed dolomite coarse aggregate (CDCA) with fully embedded IPE steel sections under axial compressive loads. Based on the sensitivity analysis, it can be concluded that the behavior of the CDCA concrete can be captured well using the data and factors of the normal general concrete. Theoretical calculations were conducted using nine available codes (YB9082-06, CECS159, Hong Kong code, ECP203, ECP-LRFD, ACI318M, AISC-360-16, BS-5400-05, and Eurocode-4) to predict the ultimate axial capacities and compared with the experimental test and FE results. The results recommend that the effects of the parameters of the columns under axial loads should be considered for their effects on the columns' capacity, ductility, and behavior:

1. The FE analysis could accurately predict the ultimate capacity of the CCES columns. The average value of the test to FE analysis result ($P_{u,\ Test}/\ P_{u,\ FE}$) and coefficient of variation are 1.019 and 0.031, respectively, and the average value of the test to FE analysis result ($\Delta_{u,Test}/\ \Delta_{u,FE}$) and coefficient of variation are 1.036 and 0.082, respectively.
2. As CDCA concrete strength increased, the ultimate axial compression capacities increased. The average efficiency factor of almost 62% indicates that this is a good strategy for raising the P_u of this kind of specimen, especially considering the cost of raising the f_{cu}. The post-ultimate behaviors of the studied specimens with f_{cu} greater than 50 MPa show a rapid decline in the strength capacity, indicating occurrences of brittle collapses. Increasing the f_{ss} strategy is not very effective and gives brittle behavior, which is attributed to the increasing carbon percentage as the steel strength grade increases, which results in increasing the stiffness and decreasing the elongation deformability of steel, even though enhancing the f_{ss} slightly improves the specimens' capacity.
3. As the ρ_{sv} increased from 0.59% to 2.36%, by about 300%, the column's capacity slightly increased by about 1.76%, caused by the tie stirrups' confinement effects on the column specimens' CDCA concrete core and IPE-shaped steel section. As ρ_{sv} was raised, the efficiency factors slightly increased. This demonstrates that this strategy is useless even though enhancing the ρ_{sv} improves the specimens' capacity and post-ultimate ductility, especially for specimens with smaller tie stirrups spacings.
4. As the ρ_{sl} ratios increased, the column's capacity increased. When the ρ_{sl} was raised from 1.64 to 4.19% by about 155.49%, the column's capacity increased by about 17.63%. This was caused by the effects of the larger value of steel ratio participating in bearing the load of the column specimens. The efficiency factors slightly decreased as ρ_{sl} increased, and the average efficiency factor was almost 12%.
5. The SCs/studs spacings effect is insignificant in the CCES columns with CDCA concrete under axial load. Using the SCs system technique made from steel reinforcement bars and stud SCs (with head and shank) welded to a flange of steel-shaped CDCA concrete increases the columns' capacity by an average value of about 4.9% of the control specimen without SCs. The columns' capacity increased by average values of 4.06%, 7.00%, and 3.65% for the series of specimens SCØ8, SCØ10, and studØ10, respectively.
6. The ultimate capacities were predicted using nine available codes (AISC-360-16, (2016); BS.5400-5, 2002; Eurocode-4, 2004; ACI318M-14, 2014; ECP-SC-LRFD, 2012; YB9082-06, 2007; ECP-203, 2018; CECS-230-, 2008, 2009; Code-11, 2011) to design the columns using the traditional methods and to determine whether applying these methods on CCES col-

Table 11 The comparison between predicted to test and FE results

Specimen number	*Test to calculated ultimate capacity, kN*								
	$P_{ut,Test}/P_{uo,YB}$	$P_{ut,Test}/P_{uo,CECS}$	$P_{u,FE}/P_{uo,Hong\ Kong}$	$P_{ut,Test}/P_{uo,ECP203}$	$P_{ut,Test}/P_{uo,ECP-LRFD}$	$P_{ut,Test}/P_{uo,ACI}$	$P_{ut,Tes}/P_{uo,AISC}$	$P_{ut,Test}/P_{uo,BS}$	$P_{ut,Test}/P_{uo,EC4}$
Specimen #1	1.21	1.39	1.56	1.33	1.61	1.41	1.40	1.59	1.23
Specimen #2	1.21	1.40	1.57	1.33	1.62	1.41	1.40	1.60	1.23
Specimen #3	1.31	1.51	1.69	1.44	1.74	1.52	1.51	1.72	1.32
Specimen #4	1.31	1.51	1.69	1.44	1.74	1.52	1.51	1.72	1.32
Mean	1.26	1.45	1.63	1.38	1.68	1.46	1.46	1.66	1.28
Standard deviation	0.048	0.055	0.062	0.053	0.064	0.056	0.056	0.063	0.049
Coef. of var. = stand. dev./mean	0.038	0.038	0.038	0.038	0.038	0.038	0.038	0.038	0.038
Specimen number	*FE to calculated ultimate capacity, kN*								
	$P_{u,FE}/P_{uo,YB}$	$P_{u,FE}/P_{uo,CECS}$	$P_{u,FE}/P_{uo,Hong\ Kong}$	$P_{u,FE}/P_{uo,ECP20}$	$P_{u,FE}/P_{uo,ECP-LRFD}$	$P_{u,FE}/P_{uo,ACI}$	$P_{u,FE}/P_{uo,AISC}$	$P_{u,FE}/P_{uo,BS}$	$P_{u,FE}/P_{uo,EC4}$
Specimen #1	1.22	1.41	1.58	1.34	1.63	1.42	1.414	1.614	1.240
Specimen #2	1.22	1.40	1.58	1.34	1.62	1.42	1.409	1.608	1.236
Specimen #3	1.25	1.44	1.62	1.37	1.67	1.45	1.446	1.650	1.268
Specimen #4	1.25	1.44	1.62	1.37	1.66	1.45	1.444	1.648	1.266
Mean	1.23	1.42	1.60	1.36	1.65	1.44	1.428	1.630	1.253
Standard deviation	0.014	0.017	0.019	0.016	0.019	0.017	0.017	0.019	0.015
Coef. of var. = stand. dev./mean	0.012	0.012	0.012	0.012	0.012	0.012	0.012	0.012	0.012

umns with CDCA concrete under axial load would be feasible. The codes calculations give conservative results. The Chinese code, YB9082-06 [9], provides the closest calculated ultimate capacity of the columns to both the test and FE results. The findings produced by the Egyptian code of steel, ECP-LRFD (ECP-SC-LRFD, 2012), are the most conservative.

Acknowledgements
The author acknowledges the financial support of the open access funding provided by The Science, Technology & Innovation Funding Authority (STDF) in cooperation with The Egyptian Knowledge Bank (EKB).

Author Contributions
MM.A.M: conceptualization, investigation, formal analysis, resources, software, data curation, methodology, validation, visualization, writing—original draft preparation, writing—review and editing.

Funding
Open access funding provided by The Science, Technology & Innovation Funding Authority (STDF) in cooperation with The Egyptian Knowledge Bank (EKB).

Availability of Data and Materials
All data are available on request.

Declarations

Competing interests
The author declares no conflict regarding this manuscript's study, authorship, and/or publication.

Author details
[1]Civil Engineering Department, Faculty of Engineering, Al-Azhar University, Qena, Egypt.

Received: 27 March 2023 Accepted: 6 September 2023
Published online: 24 January 2024

References

ACI318M-14. (2014). *Building code requirements for structural concrete and commentary*. Farmington Hills: American Concrete Institute.
AISC-360-16. (2016). *Specification for structural steel buildings Chicago*. Illinois: American Institute for Steel Construction.
Alharthi, Y. M., Sharaky, I. A., Elamary, A. S., Al-Sharef, A., Al-Salmi, A., Al-Sufyani, A., et al. (2022). Flexural behavior and capacity of composite

concrete-steel beams using various shear connectors. *Arabian Journal for Science and Engineering*. https://doi.org/10.1007/s13369-022-07485-y
Begum, M., Driver, R. G., & Elwi, A. E. (2013). Behaviour of partially encased composite columns with high strength concrete. *Engineering Structures, 56*, 1718–1727. https://doi.org/10.1016/j.engstruct.2013.07.040
Berke, P. Z., & Massart, T. J. (2018). Modelling of stirrup confinement effects in RC layered beam finite elements using a 3d yield criterion and transversal equilibrium constraints. *International Journal of Concrete Structures and Materials, 12*(1), 49. https://doi.org/10.1186/s40069-018-0278-z
BS.5400-5. (2002). *Steel, concrete and composite bridges; Part 5: Code of Practice for Design of Composite Bridges*. London: BSI publications.
CECS-230-2008. (2009). *Specification for design of steel-concrete mixed structure of tall buildings*. Beijing: China Planning Press.
Chen, Y., Zhu, L., & Yang, Y. (2022). Test study of precast SRC column under combined compression and shear loading. *Steel and Composite Structures, 42*(2), 265–275. https://doi.org/10.12989/scs.2022.42.2.265
Code-11, H. (2011). *Code of practice for the structural use of steel 2011*. Hong Kong: Buildings Department.
Du, Y., Zhou, H., Jiang, J., & Liew, J. R. (2021). Behaviour of ultra-high strength concrete encased steel columns subject to ISO-834 fire. *Steel and Composite Structures, 38*(2), 121. https://doi.org/10.12989/scs.2021.38.2.121
ECP-203. (2018). *Egyptian code of practice for design and construction of concrete structures*. Cairo: Housing and Building National Research Center (HBRC).
ECP-SC-LRFD. (2012). *Egyptian code of practice for steel construction*. Cairo: Housing and Building National Research Center (HBRC).
Ellobody, E., & Young, B. (2011). Numerical simulation of concrete encased steel composite columns. *Journal of Constructional Steel Research, 67*(2), 211–222. https://doi.org/10.1016/j.jcsr.2010.08.003
Ellobody, E., Young, B., & Lam, D. (2011). Eccentrically loaded concrete encased steel composite columns. *Thin-Walled Structures, 49*(1), 53–65. https://doi.org/10.1016/j.tws.2010.08.006
Eurocode-4. (2004). *Design of composite steel and concrete structures, part 11: general rules and rules for buildings (BS-EN1994–1–1)*. London: British Standards Institution.
Han, Q., Wang, Y., Xu, J., Xing, Y., & Yang, G. (2017). Numerical analysis on shear stud in push-out test with crumb rubber concrete. *Journal of Constructional Steel Research, 130*, 148–158. https://doi.org/10.1016/j.jcsr.2016.12.008
Hui, C., Zhang, F., Zhang, Z., Liu, X., Hai, R., & Myers, J. J. (2020). Research on the compression behavior of steel reinforced concrete columns with built-in steel tubes. *International Journal of Steel Structures, 20*(4), 1319–1326. https://doi.org/10.1007/s13296-020-00367-9
Khan, M. K. I., Lee, C. K., & Zhang, Y. X. (2020). Numerical modelling of engineered cementitious composites-concrete encased steel composite columns. *Journal of Constructional Steel Research, 170*, 106082. https://doi.org/10.1016/j.jcsr.2020.106082
Lai, B., & Liew, J. Y. R. (2021). Investigation on axial load-shorting behaviour of high strength concrete encased steel composite section. *Engineering Structures, 227*, 111401. https://doi.org/10.1016/j.engstruct.2020.111401
Lai, B., Liew, J. R., & Wang, T. (2019a). Buckling behaviour of high strength concrete encased steel composite columns. *Journal of Constructional Steel Research, 154*, 27–42. https://doi.org/10.1016/j.jcsr.2018.11.023
Lai, B., Richard Liew, J. Y., & Wang, T. (2019b). Buckling behaviour of high strength concrete encased steel composite columns. *Journal of Constructional Steel Research, 154*, 27–42. https://doi.org/10.1016/j.jcsr.2018.11.023
Li, W., & Cai, Y.-X. (2019). Performance of CFDST stub columns using high-strength steel subjected to axial compression. *Thin-Walled Structures, 141*, 411–422. https://doi.org/10.1016/j.tws.2019.04.021
Lin, J., Wang, J., & Xu, R. (2014). Cohesive zone model based numerical analysis of steel-concrete composite structure push-out tests. *Mathematical Problems in Engineering*. https://doi.org/10.1155/2014/175483
Liu, D., Wang, F., & Fu, F. (2018). Experimental research on the shear connectors in foam concrete with C-channel embedment. *International Journal of Concrete Structures and Materials, 12*(1), 51. https://doi.org/10.1186/s40069-018-0281-4
Mander, J. B., Priestley, M. J. N., & Park, R. (1988a). Observed stress-strain behavior of confined concrete. *Journal of Structural Engineering, 114*(8), 1827–1849. https://doi.org/10.1061/(ASCE)0733-9445(1988)114:8(1827)
Mander, J. B., Priestley, M. J. N., & Park, R. (1988b). Theoretical stress-strain model for confined concrete. *Journal of Structural Engineering, 114*(8), 1804–1826. https://doi.org/10.1061/(ASCE)0733-9445(1988)114:8(1804)
Mostafa, M. M. A. (2016). *The effect of confinement and shear connectors on the ultimate capacity of the short composite column*. Al-Azhar University.
Mostafa, M. M. A., Chen, S., Wu, T., Liu, X., & Liu, Y. (2022a). Experimental seismic analysis of new types of steel-reinforced lightweight concrete columns with cross-shaped steel section. *Journal of Building Engineering, 60*, 105202. https://doi.org/10.1016/j.jobe.2022.105202
Mostafa, M. M. A., Wu, T., & Fu, B. (2021). Axial behavior of steel reinforced lightweight aggregate concrete columns: Analytical studies. *Steel and Composite Structures, 38*(2), 223–239.
Mostafa, M. M. A., Wu, T., & Liu, X. (2022b). Bond-slip behaviors of composite steel-reinforced high strength lightweight aggregate concrete columns with innovative X-shaped steel sections. *Construction and Building Materials*. https://doi.org/10.1016/j.conbuildmat.2022.127838
Mostafa, M. M. A., Wu, T., Liu, X., & Fu, B. (2019). The composite steel reinforced concrete column under axial and seismic loads: A review. [SharedIt link:: https://rdcu.be/bLnYJ]. *International Journal of Steel Structures, 19*(6), 1969–1987. https://doi.org/10.1007/s13296-019-00257-9
Pereiraa, M. F., De Nardin, S., & El Debs, A. L. (2016). Structural behavior of partially encased composite columns under axial loads. *Steel and Composite Structures, 20*(6), 1305–1322.
Soliman, K. Z., Arafa, A. I., & Elrakib, T. M. (2013). Review of design codes of concrete encased steel short columns under axial compression. *HBRC Journal, 9*(2), 134–143. https://doi.org/10.1016/j.hbrcj.2013.02.002
Štefan, R., Sura, J., Procházka, J., Kohoutková, A., & Wald, F. (2019). Numerical investigation of slender reinforced concrete and steel-concrete composite columns at normal and high temperatures using sectional analysis and moment-curvature approach. *Engineering Structures, 190*, 285–305. https://doi.org/10.1016/j.engstruct.2019.03.071
Sun, D., Yang, Y., Xue, Y., Yu, Y., An, K., & Chen, Y. (2021). Seismic performance of RC columns with encased prefabricated high-strength CFST core. *Steel and Composite Structures, 39*(6), 723–736. https://doi.org/10.12989/scs.2021.39.6.723
Sun, Y., Liu, Y., Wu, T., Liu, X., & Lu, H. (2019). Numerical analysis on flexural behavior of steel fiber-reinforced LWAC beams reinforced with GFRP bars. *Applied Sciences, 9*(23), 5128. https://doi.org/10.3390/app9235128
Tunc, G., Dakhil, A., & Mertol, H. C. (2021). Experimental analysis of the behavior of composite column-reinforced concrete beam joints. *Arabian Journal for Science and Engineering, 46*(11), 10785–10801. https://doi.org/10.1007/s13369-021-05545-3
Venkateshwaran, A., Lai, B., & Liew, J. Y. R. (2021). Design of steel fiber-reinforced high-strength concrete- encased steel short columns and beams. *ACI Structural Journal*. https://doi.org/10.14359/51728077
Venkateshwaran, A., Lai, B.-L., & Liew, J. Y. R. (2022). Buckling resistance of steel fibre-reinforced concrete encased steel composite columns. *Journal of Constructional Steel Research, 190*, 107140. https://doi.org/10.1016/j.jcsr.2022.107140
Xue, Y., Yang, Y., & Yu, Y. (2020a). Pseudostatic testing for load-carrying capacity of precast concrete-encased steel composite columns. *Journal of Building Engineering*. https://doi.org/10.1016/j.jobe.2020.101189
Xue, Y., Yang, Y., & Yu, Y. (2020b). Shear strength model for steel reinforced concrete composite members: Short columns and deep beams. *Engineering Structures, 216*, 110748. https://doi.org/10.1016/j.engstruct.2020.110748
Yang, Y., Chang, H., & Wang, C. (2021a). Study on post-fire performance and residual capacity of steel reinforced high-strength concrete composite columns under eccentric compression. *IOP Conference Series: Earth and Environmental Science, 676*(1), 012075. https://doi.org/10.1088/1755-1315/676/1/012075
Yang, Y., Chen, X., Xue, Y., Yu, Y., & Zhang, C. (2021b). Shear behavior of concrete-encased square concrete-filled steel tube members: experiments and strength prediction. *Steel and Composite Structures, 38*(4), 431–445. https://doi.org/10.12989/scs.2021.38.4.431
Yang, Y., Chen, Y., Zhang, W., & Feng, S. (2019a). Behavior of partially precast steel reinforced concrete columns under eccentric loading. *Engineering Structures, 197*, 109429. https://doi.org/10.1016/j.engstruct.2019.109429
Yang, Y., & Li, H. (2020). Experimental study on shear behaviors of partial precast steel reinforced concrete beams. *Steel and Composite Structures, 37*(5), 605–620. https://doi.org/10.12989/scs.2020.37.5.605
Yang, Y., Xue, Y., Yu, Y., & Gong, Z. (2019b). Post-fire test of precast steel reinforced concrete stub columns under eccentric compression. *Steel and Composite Structures, 33*(1), 111–122. https://doi.org/10.12989/scs.2019.33.1.111

YB9082-06. (2007). *Technical specification for steel reinforced concrete structure (national standards of People's Republic of China)*. Beijing: Metallurgical Industry Press.
Yu, Y., Yang, Y., Xue, Y., & Liu, Y. (2020). Shear behavior and shear capacity prediction of precast concrete-encased steel beams. *Steel and Composite Structures, 36*(3), 261–272. https://doi.org/10.12989/scs.2020.36.3.261
Zhang, S., Miao, K., Wei, Y., Xu, X., Luo, B., & Shi, W. (2023). Experimental and theoretical study of concrete-filled steel tube columns strengthened by FRP/steel strips under axial compression. *International Journal of Concrete Structures and Materials*. https://doi.org/10.1186/s40069-022-00556-2
Zhao, Q., Du, Y., Peng, Y., Xu, C., & Huang, G. (2020). Shear performance of short channel connectors in a steel-UHPC composite deck. *International Journal of Steel Structures, 20*(1), 300–310. https://doi.org/10.1007/s13296-019-00289-1

Publisher's Note

Mostafa M. A. Mostafa Lecturer at Civil Engineering Department, Faculty of Engineering, Al-Azhar University, Qena 83513, Egypt